Phase Equilibria of a Mixture of Side-Chain Liquid Crystalline Polymer and Low Molecular Mass Liquid Crystal

Namil Kim,[†] Jaehyuck Choi,[†] Liang-Chy Chien,[‡] and Thein Kyu*,[†]

Department of Polymer Engineering, University of Akron, Akron, Ohio 44325-0301, and Liquid Crystal Institute, Kent State University, Kent, Ohio 44242

Received August 21, 2007; Revised Manuscript Received October 23, 2007

ABSTRACT: A side-chain liquid crystalline polymer based on *p*-methoxyphenyl-*p*′-acryloyloxy benzoate was synthesized for utilization in a polymer dispersed liquid crystal. Phase diagram of the blends of side-chain liquid crystalline polymer and low molecular mass liquid crystal (K21) was established by means of light scattering and differential scanning calorimetry. A theoretical phase diagram was established by self-consistently solving the combined free energy densities of Flory−Huggins, Maier−Saupe, and phase field theory of solidification. The theoretical phase diagram was established to compare with the observed phase diagram of the binary mesogenic mixtures, showing the isotropic, isotropic + nematic ($L_1 + N_2$), nematic + nematic ($N_1 + N_2$), and crystal + nematic ($Cr_1 + N_2$) coexistence regions. The morphologies of these coexistence regions were further confirmed by polarized optical microscopy.

Introduction

Polymer dispersed liquid crystals (PDLC) and polymer stabilized liquid crystals (PSLC) have gained considerable interest for their applications for switchable windows and reflective displays. The former contains less than 50% LC, whereas the latter is composed of >95% LC concentration in the polymer matrix. PDLC is made up of micron-sized liquid crystal droplets that are dispersed in an isotropic polymer matrix.[1−4] PDLC films are generally prepared via phase separation either by polymerization-induced phase separation (PIPS) or by thermal quenching from a homogeneous solution. In the former, PIPS permits tailoring of liquid crystal dispersions and ultimately electro-optic properties through control of the competition between phase separation dynamics and the rate of polymerization.[5,6] In the case of thermally induced phase separation (TIPS), droplet size can be controlled by thermal quenching or slow cooling.[7,8] It is well documented that switching voltage, response time, brightness, and contrast of PDLCs displays depend on the resulting morphology and dispersion of liquid crystal droplets, and thus understanding thermodynamics of phase equilibrium is of paramount importance to gain control of the emerged domain structures of the PDLC films.

In our previous studies,[9−12] various phase diagrams of SCLCP/LC composites have been established experimentally and theoretically on the basis of the combined free energy of Flory−Huggins (FH) theory for isotropic mixing, Maier−Saupe (MS) theory for nematic, and Maier−Saupe−McMillan (MSM) theory for smectic ordering. However, the issues of crystal−mesophase or crystal−isotropic phase transitions, if any, were not addressed in the free energy descriptions.

In the present study, SCLCP was synthesized from *p*-methoxyphenyl-*p*′-acryloyloxy benzoate monomer for use as polymer matrix in the PDLC films. The binary phase diagram of the as-synthesized SCLCP and low molecular mass liquid crystal (K21) was determined by means of light scattering (LS) and differential scanning calorimetry (DSC). In modeling of the present system, the phase field free energy (PF) of crystal solidification of small molecule LC was incorporated in the total free energy of the SCLCP/LC system. The theoretical coexistence curves were calculated by solving self-consistently the combined FH/MS/PF free energies, and the results were tested with the experimental phase diagram. The predicted coexistence regions were further confirmed experimentally by means of polarized optical microscopy (POM).

Experiments

Synthesis of SCLCP. Several synthesis schemes for *p*-alkoxyphenyl-*p*′-acryloyloxy benzoate monomer were developed by several research groups.[13−15] The synthesis steps consist of introducing a flexible spacer via etherification followed by esterification to introduce polymerizable double bonds. Even though the monomer thus synthesized by the above schemes can be polymerized to form a side-chain liquid crystalline polymer, the problem of low yield was encountered, e.g., 51% by Ringsdorff's group[13] and 50% by Hardy's group.[14] The synthesis scheme adopted here was different from the reported ones[13,14] in that the spacer group was introduced in the last step. The present methodology is advantageous because the introduction of spacer length does not affect the reaction scheme, while giving a high yield. The monomer was synthesized via four steps: (a) synthesis of ethyl-*p*-benzyloxy benzoate; (b) synthesis of *p*-benzyloxybenzoic acid; (c) synthesis of *p*-methoxyphenyl-*p*′-benzyloxy benzoate; and (d) synthesis of *p*-methoxyphenyl-*p*′-acryloyloxy benzoate (Scheme 1).

Blend Preparation and Characterization. Gel permeation chromatography (GPC) experiments were carried out using an HPLC pump (Waters 510) and a refractometer (Water 410). The number-average and weight-average molecular weights of the SCLCP were 54 000 and 165 000, respectively, with a polydispersity of 3.03. Thermal analysis of the mixtures was performed using a Perkin-Elmer DSC-7. During the experiment, the chamber was maintained under the circulating N_2 atmosphere at a flow rate of 30 mL/min. Temperature calibration was performed using an indium standard having a melting point of 165.5 °C. An optical microscope (Nikon, Pol-12) equipped with a 35 mm camera (FX-35DX, Nikon) and a hot stage (Mettler FP82 HT) interlinked with a programmable temperature controller (Mettler Toledo FP90 processor) were used for polarized optical microscopy (POM) experiments.

Low molecular weight liquid crystal (LMWLC) used in this study is a single-component nematic liquid crystal, 4-*n*-heptyl-4-cyano-

* Corresponding author. E-mail: tkyu@uakron.edu.
[†] University of Akron.
[‡] Kent State University.

10.1021/ma0718898 CCC: $37.00
Published on Web 11/29/2007

Scheme 1. Synthesis Scheme of *p*-Methoxyphenyl-*p'*-acryloyloxy Benzoate Monomer and Chemical Structure of Side-Chain Liquid Crystalline Polymer along with the Indicated Yields at Each Step

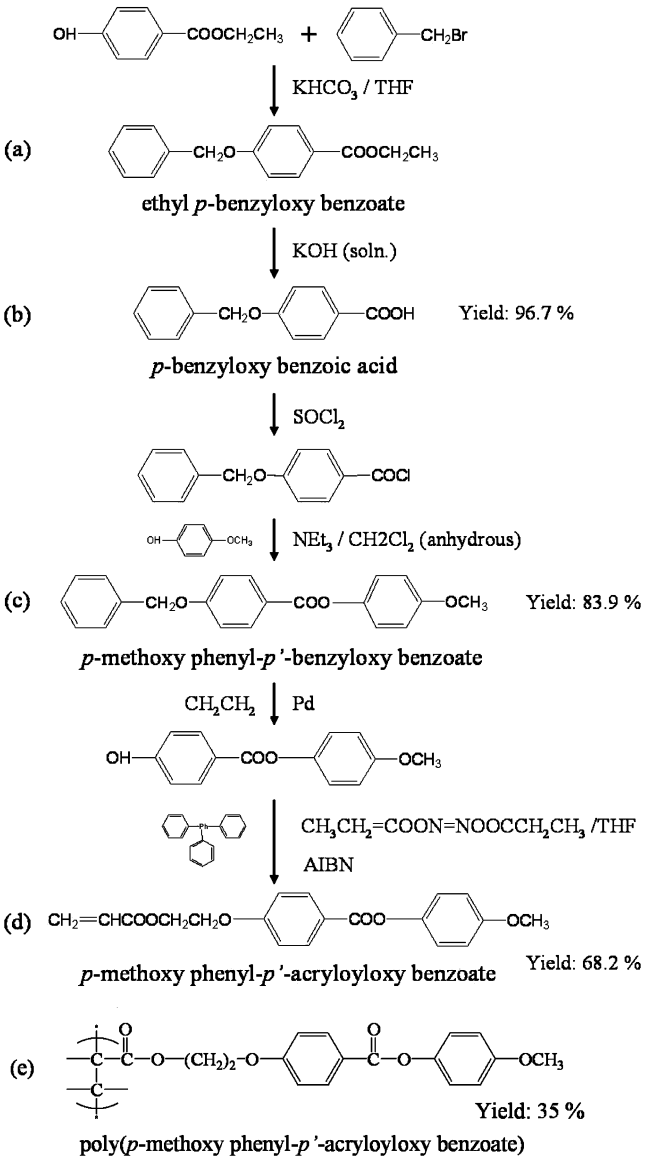

biphenyl (K21, alternatively known as 7CB having $T_{KN} = 30$ °C and $T_{NI} = 42$ °C), which was purchased from Merck Inc. The K21 was mixed with the as-synthesized SCLCP matrix, i.e., poly(*p*-methoxyphenyl-*p'*-acryloyloxy benzoate) ($T_g = 65$ °C and $T_{NI} = 120$ °C), by dissolving in a common solvent, tetrahydrofuran (THF), at room temperature. A drop of the K21/SCLCP solution was spread on a glass slide to form a thin film (about 10 μm thick). This sample was dried in a vacuum oven at 60 °C for 3 days to remove any residual solvent for use in light scattering, optical microscopy, and DSC experiments.

Light scattering experiments were carried out by monitoring the scattered intensity at a given scattering angle (~20°) using a silicon photodiode detector (HC-220-01, Hamamatsu Co.). A randomly polarized He−Ne laser (LSR2R, Aerotech) with a wavelength of 632.8 nm was used as an incident light source. A heating chamber equipped with a programmable temperature controller (model CN-2012, Omega) was used for temperature scans. The heating and cooling rates were 1 °C/min unless indicated otherwise.

Model Descriptions

The free energy of SCLCP/K21 mixtures can be described in terms of a combined Flory−Huggins (g^{FH}), Maier−Saupe (g^{MS}), and phase field (g^{PF}) theory, viz., $g = g^{FH} + g^{MS} + g^{PF}$. The free energy density of Flory−Huggins for isotropic mixing is expressed as[16,17]

$$g^{FH} = \frac{G^{FH}}{nkT} = \frac{\phi_1}{r_1}\ln\phi_1 + \frac{\phi_2}{r_2}\ln\phi_2 + \chi_{FH}\phi_1\phi_2 \qquad (1)$$

where subscripts 1 and 2 refer to LMWLC and SCLCP and kT represents thermal energy with k being the Boltzmann constant and n the number of molecules. r_1 and r_2 representing the number of lattice sites occupied by respective components can be related to volume fractions $\phi_1$and ϕ_2 through $\phi_1 = n_1r_1/n_1r_1 + n_2r_2$ and $\phi_2 = n_2r_2/n_1r_1 + n_2r_2$. The FH interaction parameter χ_{FH} representing amorphous−amorphous interaction between the pair is generally assumed to be inversely proportional to the absolute temperature, i.e., $\chi_{FH} = A + B/T$, where A is related to athermal entropic correction and B represents enthalpic contribution.

The free energy density of nematic ordering can be described according to Maier−Saupe mean-field theory.[18−20]

$$g^{MS} = \frac{G^{MS}}{nkT} = -\sum\nolimits_1\phi_1 - \sum\nolimits_2\phi_2 - \frac{1}{2}\nu_{11}s_1^2\phi_1^2 - \frac{1}{2}\nu_{22}s_2^2\phi_2^2 - \nu_{12}s_1s_2\phi_1\phi_2 \qquad (2)$$

The first two terms indicate the decrease of entropy, and the last three terms represent enthalpic contribution to the total free energy. s_1 and s_2 are orientational order parameters, and ν_{11} and ν_{22} represent the nematic interaction parameters of the pure constituents which can be expressed as

$$\sum\nolimits_j = -\int f(\theta_j)\ln[4\pi f(\theta_j)]\,d\Omega_j = \ln Z_j - m_j s_j \qquad (3)$$

$$s_j = \int f(\theta_j)\frac{1}{2}(3\cos^2\theta_j - 1)\,d\cos\theta_j = \frac{1}{Z_j}\frac{dZ_j}{dm_j} \qquad (4)$$

with

$$\nu_{11} = 4.541\frac{T_{NI,1}}{T}, \quad \nu_{22} = 4.541\frac{T_{NI,2}}{T} \qquad (5)$$

in which m_j and Z_j are dimensionless mean field strength and partition function, respectively. By minimizing the free energy with respect to the orientational order parameters, the mean field parameters (m_j) can be related to the order parameters (s_1, s_2) and the anisotropic interaction parameters (ν_{11}, ν_{22}, ν_{12}), i.e., $m_1 = \nu_{11}s_1\phi_1 + \nu_{12}s_2\phi_2$ and $m_2 = \nu_{22}s_2\phi_2 + \nu_{12}s_1\phi_1$. Inserting these m_j into eq 2 leads to

$$g^{MS} = -\phi_1\ln Z_1 - \phi_2\ln Z_2 + \frac{1}{2}\nu_{11}s_1^2\phi_1^2 + \frac{1}{2}\nu_{22}s_2^2\phi_2^2 + \nu_{12}s_1s_2\phi_1\phi_2 \qquad (6)$$

The cross-interaction parameter ν_{12} is evaluated in the context of the geometric mean approach, i.e.

$$\nu_{12} = c_\nu\sqrt{\nu_{11}\nu_{22}} \qquad (7)$$

where c_ν signifies the departure from the ideal geometric mean, characterizing the relative strength of the cross-interaction between the two dissimilar mesogens relative to that in the same species.

Regarding the free energy of crystal solidification, a phase field model pertaining to Landau-type asymmetric potential[21−24] may be utilized, i.e.

$$g^{PF} = \phi_1 f(\psi) + \chi_{ca}\phi_1\phi_2\psi^2 \tag{8}$$

$$f(\psi) = \frac{F(\psi)}{k_B T} = W\int_0^{\psi}\psi(\psi-\zeta)(\psi-1)\,d\psi$$

$$= W\left[\frac{\zeta(T)}{2}\psi^2 - \frac{\zeta(T)}{3}\psi^3 + \frac{1}{4}\psi^4\right]$$

where the crystal-phase order parameter (ψ) signifies the perfection of the crystal phase of a small molecule system; i.e., $\psi = 1$ for a perfect crystal, otherwise imperfect. In polymer crystals, it may be related to the ratio of the lamellar thickness (l) to the lamellar thickness of a perfect crystal ($l°$), viz., $\psi = l/l°$ or linear (one-dimensional) crystallinity. In a small molecule system, it is possible that the crystal can reach the equilibrium solidification potential, viz. at $\psi = 1$. The coefficients ζ and W, representing the unstable hump for the crystal nucleation to overcome the energy barrier and the penalty for the nucleation process, can be directly evaluated from the material parameters. χ_{ca} is the interaction parameter between the intracrystalline chains (in the solid phase or solvated crystals) and the isotropic polymeric solvent (i.e., amorphous chains of the second component). Note that the χ_{ca} parameter is related to the solid−liquid phase transition, whereas the conventional χ_{FH} is associated with the liquid−liquid phase separation.

Prior to calculating the coexistence lines, it is necessary to determine the mesophase or crystal−liquid phase transitions by minimizing free energy with respect to nematic (s_1, s_2) and crystal (ψ) order parameters.

$$\frac{\partial g^n}{\partial s_1} = 0 \quad \text{and} \quad \frac{\partial g^n}{\partial s_2} = 0 \quad \text{and} \quad \frac{\partial g^{PF}}{\partial \psi} = 0 \tag{9}$$

Once the solid−liquid phase transition points were known, the equilibrium coexistence points can be obtained by a double tangent method while balancing the chemical potentials in each phase. The detailed procedures for the establishment of phase diagrams involving liquid−liquid and solid−liquid phase transitions may be found elsewhere.[25]

Results and Discussion

Phase Transitions of SCLCP. The glass transition temperature of the SCLCP can be discerned around 65 °C, whereas the nematic−isotropic transition temperature appears around 120 °C (Figure 1a). In the cooling run, T_{NI} was observed at ∼115 °C. As evidenced by the disclination textures in Figure 2a, the nematic character of the SCLCP can be confirmed between T_g (65 °C) and isotropization temperature of 120 °C. As expected, K21 liquid crystals show the typical Schlieren texture (Figure 2b) between the T_{NI} of 42 °C and crystal−nematic transition temperature of 30 °C. Although the DSC data are not determined strictly under the equilibrium conditions, the SCLCP and LC (K21) utilized here are of relatively low molecular weights; thus, these experimental data should be sufficiently close to the equilibrium values.

Experimental Phase Behavior of SCLCP/LMWLC. Light scattering measurements were conducted to determine the cloud point and/or nematic−isotropic transitions. The temperature, at which a steep change in the scattered intensity curve occurs, is characterized as the phase transition point. Below T_{NI}, the PDLC film exhibits opaque appearance and scatters light, but the film becomes clear when the temperature is raised above T_{NI}. Figure 3 shows the variation of scatted intensity as a function of temperature for various concentrations. Regardless of its concentrations, all mixtures exhibit their phase transitions between those of the pure SCLCP and neat LMWLC. As for the 80 wt % of K21, the intensity drops in two steps. The higher transition temperature (58 °C) corresponds to T_{NI} of the SCLCP matrix, and the other at 40 °C is attributed to that of K21 (Figure 3a). It was found that there exists homogeneous isotropic (I), isotropic LC + nematic polymer ($L_1 + N_2$), and nematic LC + nematic polymer ($N_1 + N_2$) coexistence region in the descending order of temperature. Similar behaviors are also observed in the intermediate concentrations of K21. The mixtures having K21 concentration of less than 20 wt %, however, show only a single drop in the curve of scattered intensity with temperature (Figure 3b).

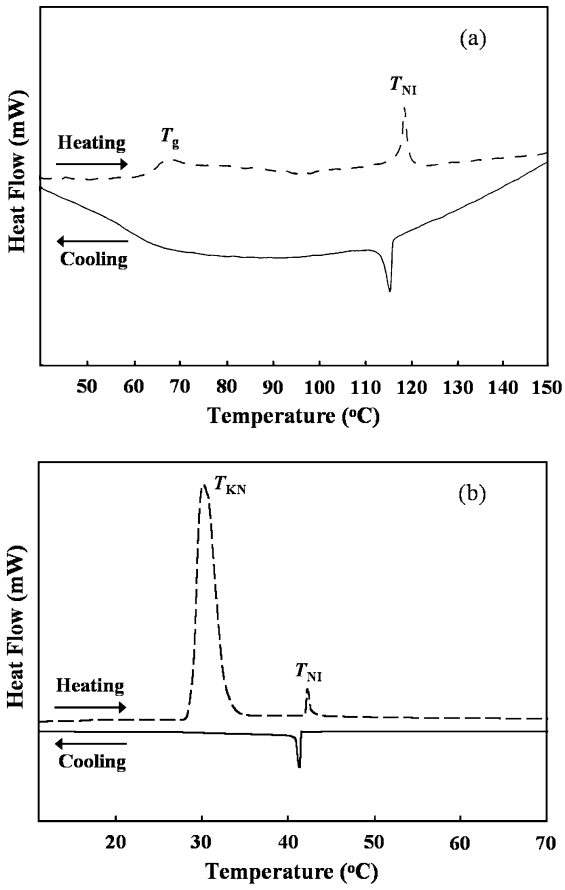

Figure 1. DSC thermograms of side-chain liquid crystalline polymer and low molecular weight liquid crystal (K21) at a heating and cooling rate of 5 °C/min: (a) SCLCP showing a glass transition at 65 °C and a nematic−isotropic transition at 120 °C; (b) pure K21 exhibiting crystal−nematic and nematic−isotropic transition at 30 and 42 °C, respectively.

Figure 4 illustrates DSC thermograms of LC and LCP mixtures obtained from the second heating cycle at a heating rate 5 °C/min. The pure K21 reveals a crystal−nematic transition around 30 °C and the nematic−isotropic transition around 45 °C in the second run (Figure 1b). The high concentrations of K21 (e.g., 90−70 wt %) show two sharp peaks around 28 and 42 °C and one broad peak (55−65 °C). The former two distinct peaks may be attributed to the crystal−nematic and nematic−isotropic transition of K21, whereas the latter broad peak is assigned to the nematic−isotropic transition of the SCLCP. The slight depression of these mesophase transition temperatures of K21 in its mixture with SCLCP may be a consequence of diluent effect caused by the nematic fluid phase of the SCLCP. As K21

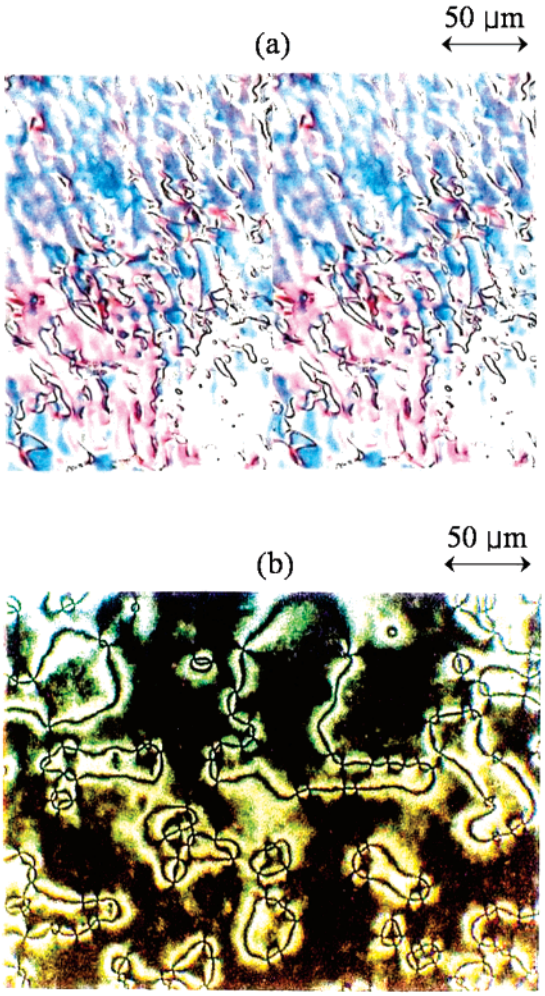

Figure 2. Optical micrographs of (a) side-chain liquid crystalline polymer (SCLCP) and (b) K21. Both materials exhibit "Schlieren" textures, which are characteristics of a nematic phase.

concentration is reduced to intermediate concentrations of 60−40 wt %, the crystal solid to nematic transition of phase-separated K21 appears in the vicinity of 28 °C, but the isotropization temperature of K21 disappears completely. However, the nematic−isotropic transition of the SCLCP, although broad, can be seen around 65 °C. Both enthalpies of crystal melting peak of K21 and nematic−isotropic phase transition of SCLCP are relatively small. Below 30 wt % K21, the DSC thermograms show only one nematic−isotropic transition peak corresponding to that of SCLCP. The crystal−nematic or nematic−isotropic phase transitions of K21 are no longer discernible. The glass transition temperature of the SCLCP located at about 65 °C has declined to 42 °C with the addition of 10 wt % of K21 due to the plasticizing effect of the LC constituent. However, the T_g seemingly disappears with further addition of K21. At the low level of <30 wt % of K21, the DSC results suggest that only one nematic phase exists. However, on the basis of DSC experiment and light scattering data, it is very difficult to analyze the trend of these experimental points or to unambiguously identify the possible coexistence regions. Hence, a theoretical phase diagram is warranted in order to identify the aforementioned coexistence phases.

Theoretical Phase Diagrams. As described earlier, the coexistence curves can be established by self-consistently solving the combined free energies of Flory−Huggins, Maier−Saupe, and phase field theory of solidification (FH/MS/PF). First, we shall determine the mesophase transition temperatures

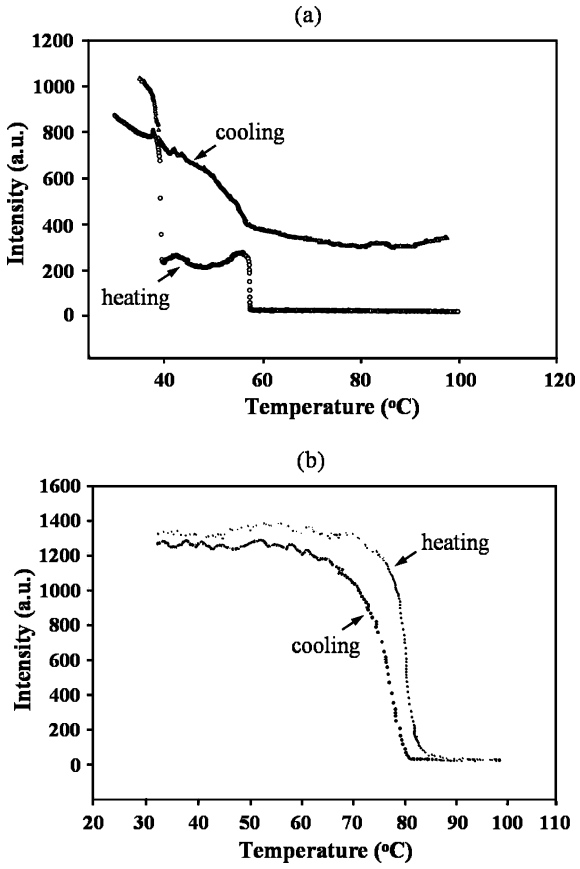

Figure 3. Laser light scattering at a heating and cooling rate 1 °C/min: (a) SCLCP/K21 = 20:80 wt % and (b) 80:20 wt %. The former shows a distinct phase transition of (I)−(L_1 + N_2)−(N_1 + N_2) in the descending order of temperature, whereas the latter exhibits only one transition (I)−(N_2).

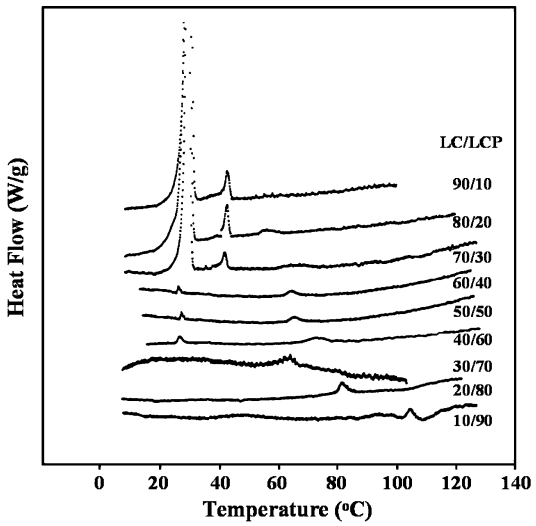

Figure 4. DSC thermograms of SCLCP/K21 mixtures at a heating rate of 5 °C/min. The high concentration of K21 reveals two peaks around 28 and 42 °C from phase-separated K21 and one broad peak from SCLCP. The mixtures containing <30 wt % K21 shows no phase separation. These DSC scans obtained from the second heating cycle.

by minimizing the total free energy with respect to the nematic order parameters (s_1, s_2) or crystal order parameter (ψ_1). Figure 5a shows the variation of the orientational order parameters as a function of temperature for different volume fractions at c_ν = 0.9. The value of c_ν smaller than unity implies that the nematics are favored to form in their neat constituents as opposed to the mixed nematic phase. According to Maier−

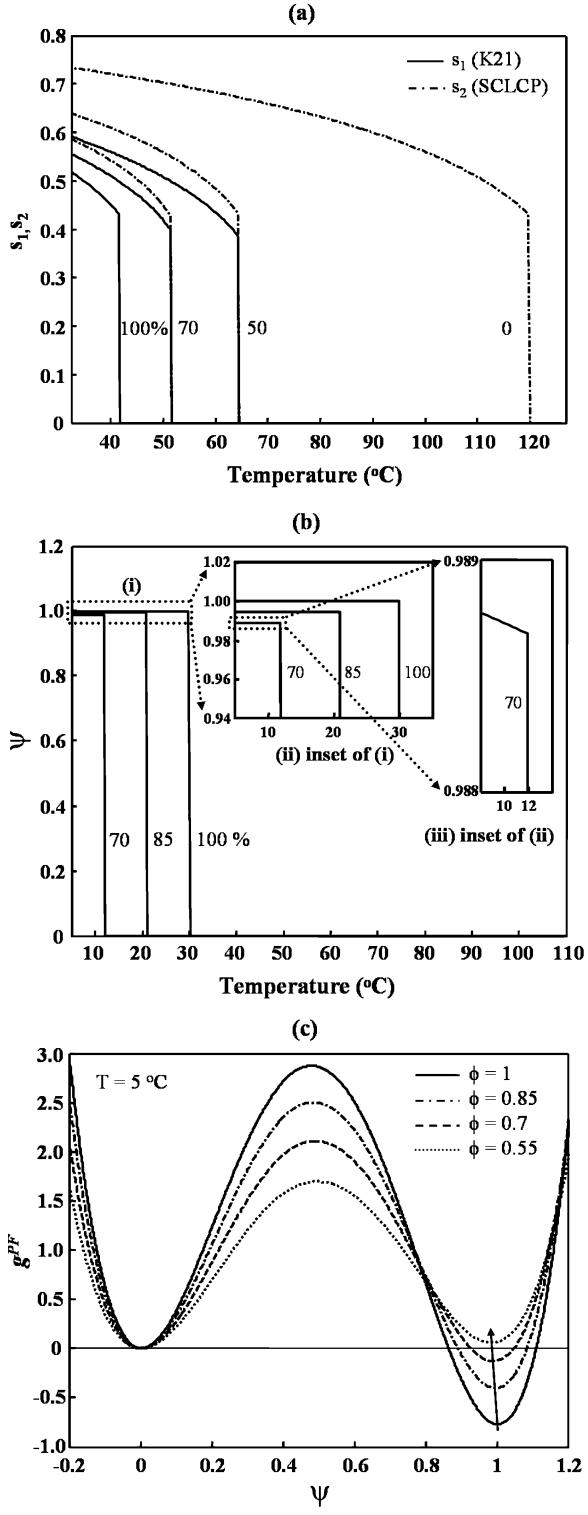

Figure 5. Order parameters of SCLCP and K21 as a function of temperature at a given composition: (a) nematic order parameters (s_1, s_2); (b) crystal order parameter (ψ); (c) concentration dependence of free energy of crystal solidification at a constant temperature (5 °C).

Saupe theory, the critical orientational order parameter is 0.429, above which the nematic ordering will take place. In Figure 5a, the nematic−isotropic transition of the pure SCLCP takes place around 120 °C, where s_2 drops discontinuously from the universal value of $s_c = 0.429$. At 50 wt % K21, minimum free energy from nematic ordering (s_2) is observed even though s_1 is lower than critical order parameter. Two separate nematic phases appear when temperature becomes lower than the T_{NI} of pure K21.

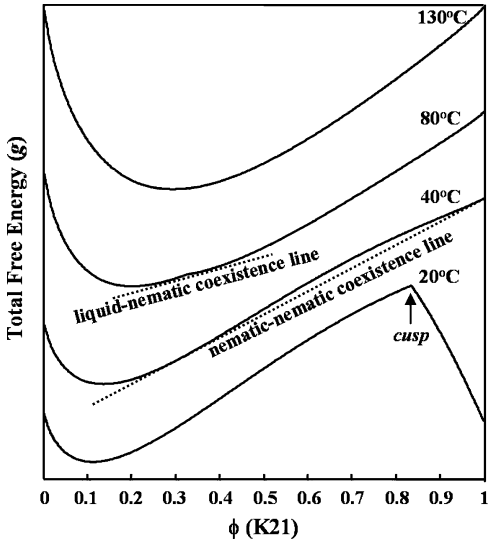

Figure 6. Total free energy curve from a combined Flory−Huggins (FH), Maier−Saupe (MS), and phase field (PF) theory of solidification and a double tangent line exhibiting phase equilibrium of ($L_1 + N_2$) and ($N_1 + N_2$).

It should be recalled that K21 crystallizes at a lower temperature. To determine the crystal−nematic phase transition, the total free energy is minimized with respect to the crystal order parameter (ψ_1), which is defined as the ratio of the lamellar thickness at a given crystallization to that of a perfect crystal. The crystal may be regarded as perfect if the value of ψ_1 is unity. The variation of ψ_1 with temperature is shown in Figure 5b. The crystal order parameter of pure K21 discontinuously declines at the crystal−nematic transition temperature (i.e., 30 °C), below which the crystallization occurs from the nematic phase. With the addition of small amount of SCLCP, the crystal order parameter becomes less than unity, suggesting that the emerged crystal is probably solvated and thus less perfect relative to the neat solid crystal. An enlarged view of 70 wt % of K21 is depicted as an inset which clearly illustrates the sharp temperature drop of the crystal order parameter.

As shown in Figure 5c, the asymmetric double well free energy curve of the neat K21 represents the isotropic melt at $\psi = 0$ and the crystal solidification at unity ($\psi = 1$). The global minimum is located at $\psi = 1$, which implies that the small molecule crystal reaches the equilibrium solidification potential well. However, the solidification potential of K21 becomes shallower with the addition of SCLCP, implying that the K21 crystallization is influenced by the polymeric solvent. When the concentration of SCLCP is 0.55, for example, the isotropic liquid phase becomes more stable than the crystal phase, as indicated by the global minimum at $\psi = 0$. It is noticed that the crystal order parameter value declines from unity with increasing SCLCP, suggesting the possible entrapment of the polymeric solvent in the crystal, i.e., the solvated crystal.

Having determined the solid−liquid phase transition and mesophase transition temperatures, the combined free energies of FH/MS/PF theory may now be minimized with respect to volume fraction of each constituent in order to calculate the coexistence lines. The changes of free energy minima at various temperatures are plotted in Figure 6. The liquid + nematic and nematic + nematic coexistence lines can be determined by balancing the chemical potentials of each phase in conjunction with the double tangent method described elsewhere.[25,26] At 130 °C, the free energy curve is a single well signifying the homogeneous (isotropic) mixture. Upon reducing to 80 °C, the free energy curve reveals a double well suggesting the nematic

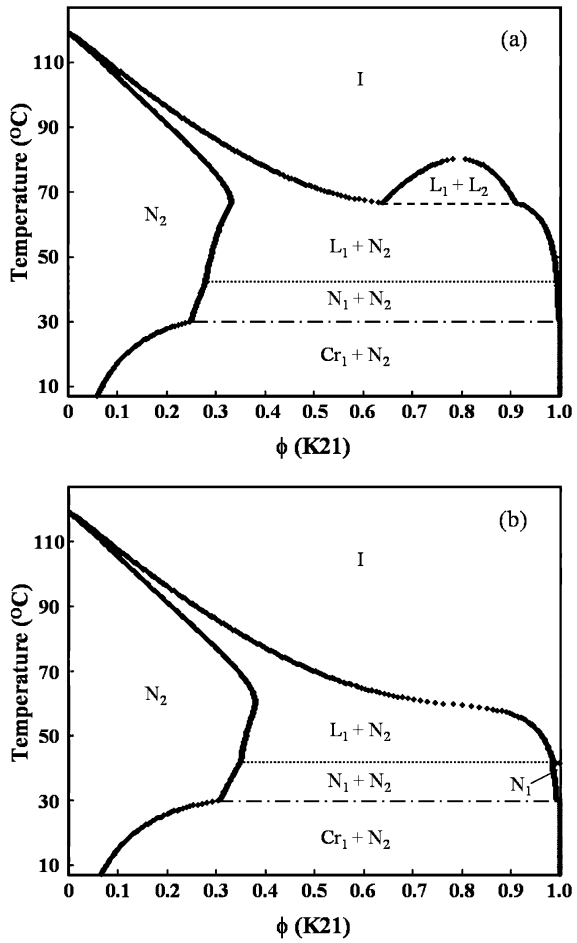

Figure 7. Effect of T_c on phase diagram of SCLCP/K21 mixtures at $c_\nu = 0.9$: (a) 80 °C and (b) 40 °C. When T_c is 80 °C, liquid−liquid equilibrium (UCST) appears with the $L_1 + N_2$ and $N_1 + N_2$ coexistence region in the intermediate concentration. On the other hand, the $L_1 + L_2$ region disappears, and a single nematic phase (N_1 and N_2) becomes more pronounced at $T_c = 40$ °C.

phase of the SCLCP in equilibrium with the isotropic liquid phase of K21. As the temperature is further reduced to 40 °C, the nematic ordering takes in both constituents, showing two minima representing the coexistence nematic + nematic phase. At 20 °C, a cusp develops in the total free energy curve; the intersection of the two free energy curves signifies the crystal−melting transition point. Similarly, the nematic + crystal coexistence point and thus its loci can be determined in terms of the double tangent approach.

It is well established in binary LC systems[11] that the c_ν value plays a critical role in determining whether nematics would form in their neat mesogens or in the mixed state. Moreover, increasing the c_ν value would expand the single phase nematic region (N), which in turn suppresses the nematic + nematic coexistence gap. Another factor that governs the shape of the phase diagram is the location of critical temperature (T_c) of the upper critical solution temperature (UCST), which can be demonstrated using a relatively weak cross-interaction condition ($c_\nu = 0.9$) under various conditions. As shown in Figure 7, at a relatively high critical temperature of 80 °C, the liquid + liquid ($L_1 + L_2$) coexistence region can be identified. In the descending order of temperature the $L_1 + N_2$ and $N_1 + N_2$ coexistence regions can be seen in a broad intermediate range of compositions. The neat N_2 region appears in the compositions having <30 wt % LC. Concurrently, a narrow $L_1 + N_2$ coexistence developed at a high temperature. Upon lowering T_c, the $L_1 + L_2$ region vanishes as it falls below the liquid + nematic line

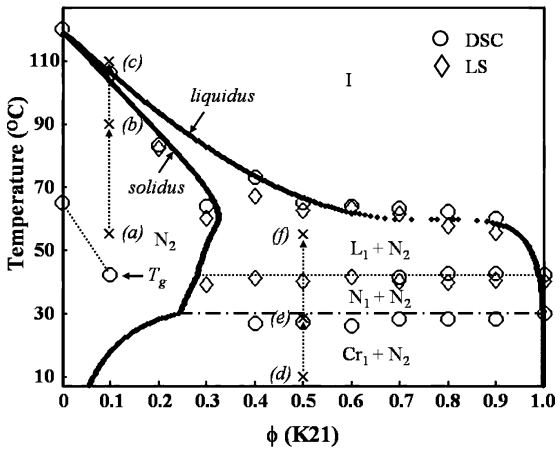

Figure 8. Theoretical and experimental phase diagram of the SCLCP/K21 system. The symbol indicates the phase transition points obtained from LS and DSC, and the solid lines represent the theoretically calculated coexistence lines intersecting with the solidus and liquidus lines.

while the single nematic phase (N_2 as well as N_1) becomes more pronounced. Meanwhile, the $L_1 + N_2$ and $N_1 + N_2$ gaps get somewhat narrower.

As pointed earlier, our cloud points and DSC results revealed various regions encompassing isotropic (I), isotropic + nematic ($L_1 + N_2$), nematic + nematic ($N_1 + N_2$) transitions. It is essential to test the validity of the present theory with the observed phase diagram of the SCLCP/K21 system. Figure 8 illustrates the temperature vs composition phase diagram obtained by the LS and DSC experiments in comparison with theory (the solid line). The material parameters used in calculation were $r_1 = 1$, $r_2 = 15$, $\chi_{FH} = 0.79$ at $T_c = 60$ °C, $T_{NI,1} = 42$ °C, $T_{NI,2} = 120$ °C, $T_{KN} = 30$ °C, and $\Delta H_1 = 22.9$ kJ/mol. W represents the penalty for overcoming the unstable potential hump. Since ζ is known for a given crystallization temperature, χ_{ca} can be estimated from the heat of fusion, ΔH_1, of K21 crystals according to $\chi_{ca} \propto W = 6[(\Delta H_1/k_B T)(1 - T/T_m^0)(1/2 - \zeta)^{-1}$; i.e., $\chi_{ca} = 0.91$ at $T = 30$ °C. Alternatively, the self-consistent solution to eq 8 can be obtained by means of the steepest descent method.[26]

As shown in Figure 8, the phase diagram of the present LC system shows no indication of liquid−liquid phase separation. Although the polydispersity of polymer is known to affect the UCST phase diagram (liquid−liquid phase separation), the effect of polydispersity is not considered here because its influence on the solid (mesophase)−liquid phase transition is insignificant. It may be inferred that the theoretical phase diagram thus calculated accords well with the experimental observation. At low K21 concentrations (<30 wt %) the neat nematic region expands, while the nematic−isotropic coexistence gap becomes narrower. In the intermediate concentrations, various coexistence phases such as isotropic liquid + nematic polymer ($L_1 + N_2$), nematic LC + nematic polymer ($N_1 + N_2$), crystal phase of LC + nematic polymer ($Cr_1 + N_2$), and single isotropic (I) and nematic polymer (N_2) were observed theoretically. These coexistence regions can be further confirmed by the optical microscopic examination.

Morphology Developments. Guided by the calculated theoretical phase diagram, the phase transition temperature and its mesomorphic texture may be identified by optical microscopy. Figure 9 shows the micrographs of 50/50 and 90/10 (SCLCP/K21) mixture obtained at a heating rate of 1 °C/min, as denoted by "×" in the phase diagram. At 50 wt % K21, the crystal structure melts into the nematic phase at 28.4 °C, showing the

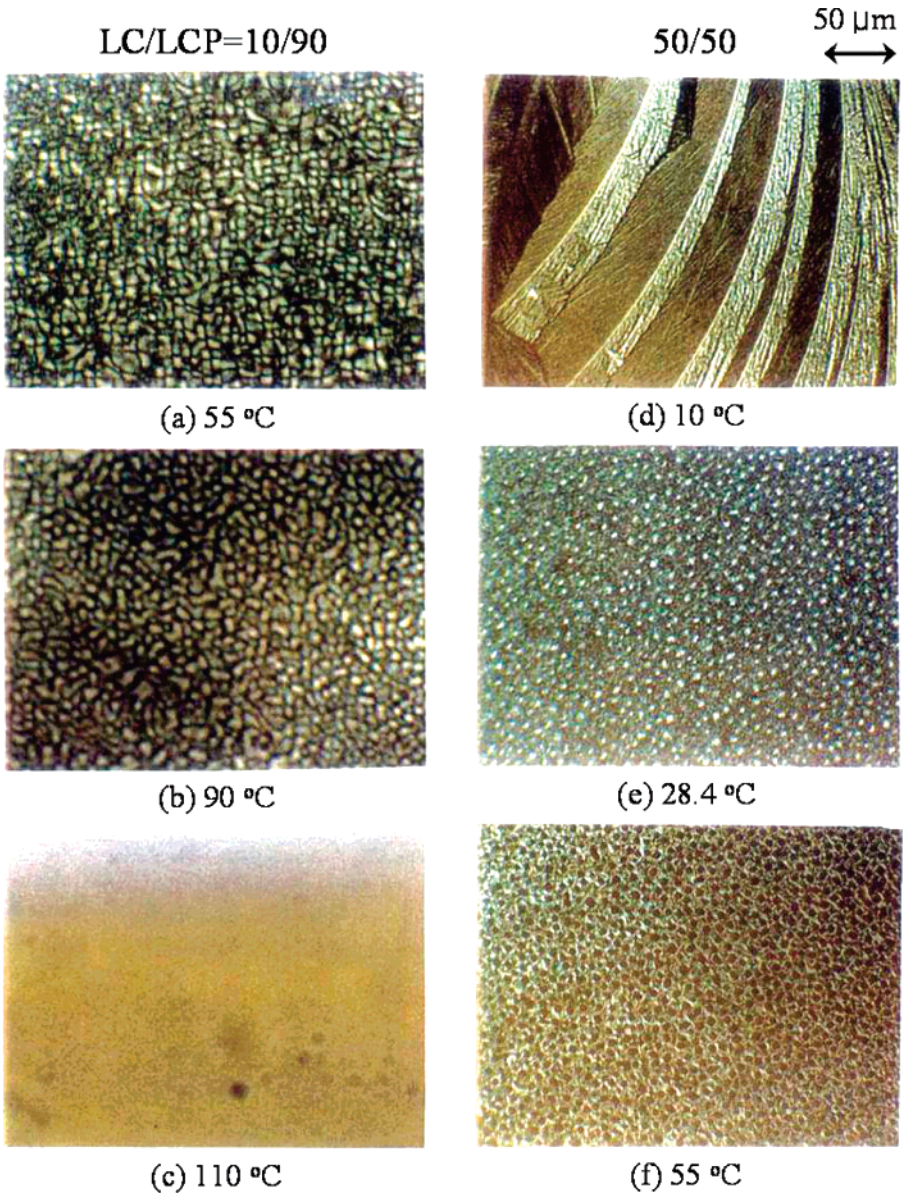

Figure 9. Optical microscopy of SCLCP/K21 mixtures at a heating rate of 1 °C/min. Pictures a−c correspond to 10 wt % K21, showing (a) and (b) the single nematic phase transforming to (c) the isotropic state (note that the narrow coexistence nematic + isotropic region was missed in this microscopic study), whereas the 50 wt % K21 shows the phase transformation from (d) crystal + nematic (the crystal structure is too dominant to discern the nematic structure) to (e) nematic + nematic and (f) nematic + isotropic phases.

phase-separated nematic domains K21 (N_1) in the continuum of the nematic SCLCP matrix (N_2). When the temperature reaches 42.5 °C, the phase-separated LC droplets (K21) transform into the isotropic melt. The isotropic region gets expanded with further increase in temperature to 55 °C as signified by the dark area. As demonstrated in the LS and DSC experiments, the mixtures containing more than 30 wt % of K21 revealed a homogeneous isotropic phase, nematic SCLCP + isotropic LC, nematic SCLCP + nematic LC, and nematic SCLCP + crystal LC. The shape of nematic droplets is governed both by the anisotropic interfacial tension between SCLCP and K21 and by the director field, which is contributed by the surface anchoring and their elastic constants.[27,28]

At low concentration of K21 (e.g., 10 wt %), the observed morphology reveals a typical Schlieren texture, characteristic of a nematic phase. This morphology changes to the isotropic phase after passing through the narrow nematic−isotropic phase transition (110 °C). It should be pointed out that the T_g of neat SCLCP appearing at 65 °C is reduced to 45 °C upon addition of 10 wt % K21 in the nematic phase. Since the T_g was suppressed below ambient temperature with further increase of K21, the nature of glassy nematics and its effect on the nematic phase diagram were not explored in detail because the gap is too narrow to find any interesting behavior (i.e., at very low K21 contents).

Conclusions

We have experimentally established the phase diagram of blends of LMWLC and SCLCP exhibiting various coexistence phases including coexistence ($L_1 + N_2$, $N_1 + N_2$, $Cr_1 + N_2$) and a single phase (N_2) regions in a manner dependent on composition and temperature. The crystal−nematic phase transition of the LMWLC in the blend with SCLCP was elucidated through the phase field model of solidification in conjunction with the Maier−Saupe model of nematic ordering. The theoretical phase diagram was constructed by self-consistently solving the combined FH/MS/PF free energies that accorded reasonably well to the observed behavior of the binary liquid crystalline polymer system. The phase transformation of mesophase structures was further demonstrated by optical microscopy in a

manner consistent with the predicted regions of the phase diagram.

Acknowledgment. Support of this work by National Science Foundation (NSF), Grant DMR-0514942, is gratefully acknowledged.

References and Notes

(1) Ma, R. Q.; Yang, D. K. *SID 97 Digest* **1997**, 101.
(2) Kato, K.; Hisaki, T.; Date, M. *Jpn. J. Appl. Phys.* **1999**, *38*, 805.
(3) Doane, J. W. In *Liquid Crystals: Applications and Uses*; Bahdur, B., Ed.; World Scientific: Singapore 1991.
(4) West. J. In *Liquid-Crystalline Polymers*; Weiss, R. A., Ober, C. K., Eds.; ACS Symp. Ser. No. 435; American Chemical Society: Washington, DC, 1990; Chapter 32, p 475.
(5) Doane, J. W.; Vaz, N. A.; Wu, B. G.; Zumer, S. *Appl. Phys. Lett.* **1986**, *48*, 269.
(6) Vaz, N. A.; Smith, G. W.; Montgomery, G. P. *Mol. Cryst. Liq. Cryst.* **1987**, *146*, 1.
(7) West, J. L. *Mol. Cryst. Liq. Cryst.* **1988**, *157*, 427.
(8) Nagaya, T.; Orihara, H.; Ishibashi, Y. *J. Phys. Soc. Jpn.* **1989**, *58*, 3600.
(9) Chiu, H.-W.; Zhou, Z. L.; Kyu, T.; Cada, L. G.; Chien, L.-C. *Macromolecules* **1996**, *29*, 1051.
(10) Chang, M.-C.; Chiu, H.-W.; Wang, X. Y.; Kyu, T.; Leroux, N.; Campbell, S.; Chien, L.-C. *Liq. Cryst.* **1998**, *25*, 733.
(11) Chiu, H.-W.; Kyu, T. *J. Chem. Phys.* **1995**, *103*, 7471.
(12) Dayal, P.; Matkar, R. A.; Kyu, T. *J. Chem. Phys.* **2006**, *124*, 224902.
(13) Finkelmann, H.; Ringsdorf, H.; Siol, N.; Wendorff, J. H. *Makromol. Chem.* **1978**, *179*, 829.
(14) Horvath, J.; Nyitrai, K.; Cser, F.; Hardy, G. *Eur. Polym. J.* **1985**, *21*, 251.
(15) Portugal, M.; Ringsdorf, H.; Zental, R. *Makromol. Chem.* **1982**, *183*, 2311.
(16) Flory, P. J. *J. Chem. Phys.***1942**, *10*, 51.
(17) Olabisi, O.; Robeson, L. M.; Shaw, M. T. *Polymer−Polymer Miscibility*; Academic: New York, 1979.
(18) Maier, W. *Z. Naturforsch., A* **1959**, *14*, 882. Maier, W.; Saupe, A. *Z. Naturforsch., A* **1960**, *15*, 287.
(19) Chandrasekhar, S. *Liquid Crystals*, 2nd ed.; Cambridge University: Cambridge, 1992.
(20) de Gennes, P. G.; Prost, J. *The Physics of Liquid Crystals*, 2nd ed.; Oxford Science: London, 1993.
(21) Harowell, P. R.; Oxtoby, D. W. *J. Chem. Phys.* **1987**, *86*, 2932.
(22) Kyu, T.; Mehta, R.; Chiu, H.-W. *Phys. Rev. E* **2000**, *61*, 4161.
(23) Xu, H.; Matkar, R.; Kyu, T. *Phys. Rev. E* **2005**, *72*, 011804.
(24) Kobayashi, R. *Physica D* **1993**, *63*, 410.
(25) Koningsveld, R.; Stockmayer, W. H.; Nies, E. *Polymer Phase Diagrams: A Textbook*; Oxford University: New York, 2001.
(26) Shen, C. S.; Kyu, T. *J. Chem. Phys.* **1995**, *102*, 556.
(27) Das, S. K.; Rey, A. D. *J. Chem. Phys.* **2004**, *121*, 9733.
(28) Francescangeli, O.; Ferrero, C.; Lucchetti, L.; Simoni, F.; Burghammer, M. *Europhys. Lett.* **2002**, *59*, 218.

MA0718898